https://doi.org/10.5194/egusphere-2026-2542
Preprint. Discussion started: 14 July 2026

tidal-insar-sim: an open-source toolkit for tide-aware ranking of NISAR L-band acquisitions over Antarctic grounding lines

Pietro Milillo[1,2,3]
[1] Department of Civil and Environmental Engineering, University of Houston, Houston, TX, USA
[2] Department of Earth and Atmospheric Science, University of Houston, Houston, TX, USA
[3] German Aerospace Centre (DLR), Microwaves and Radar Institute, Munich, Germany

Correspondence to: Pietro Milillo (pmilillo@uh.edu)

Abstract

Double-difference InSAR (DDInSAR) is the standard remote-sensing technique for mapping ice-shelf grounding lines (GLs). The signal magnitude depends on the instantaneous ocean tide at all three epochs of the rigid acquisition triplet, the SAR sensor wavelength and incidence angle, and the elastic-plate response of the floating shelf. NASA's NISAR mission, in routine Antarctic operations since the first year of service, provides the first sustained open-access L-band InSAR coverage of the ice sheet but its 12-day exact-repeat orbit closely aliases the K1 diurnal ocean tide, the dominant tidal constituent at most Antarctic GLs. We present tidal-insar-sim, an open-source Python toolkit that ingests NISAR's operational Reference Observation Plan via the live ArcGIS feature service, auto-discovers per-track acquisition UT, pass direction, frame geometry, polarisation and bandwidth from the ROP fields, evaluates the CATS2008 ocean-tide model at the exact UT of every scheduled acquisition, enumerates rigid 12-day triplets per InSAR-coherent track stream, and ranks them by predicted DDInSAR fringe count. Applied to the three Amundsen Sea Embayment grounding lines contributing most to current global mean sea-level rise (Thwaites, Pine Island, Smith) over the first year of operations (Sep 2025–Sep 2026), we find that the ROP schedules every operationally feasible track at the coast, confirming zero coastal culling, yielding 793 rigid 12-day triplets across the three GLs. Of these, only 11 % cross the 3-fringe usability threshold and only 0.6 % reach the 5-fringe excellent-quality threshold. Tide-aware ranking elevates the 87 operationally usable triplets out of the long unusable tail and, in the event of an anomaly-driven duty-cycle reduction, retains 100 % of usable yield even under 50 % culling because the operational gold is concentrated in the top quintile. The same machinery generalises to repeat-track altimetry missions targeting NASA's Surface Topography and Vegetation Designated Observable. The code (MIT license) is openly archived on Zenodo and adaptable to any SAR or altimetry constellation with a published acquisition plan.

1 Introduction

Antarctic grounding-line (GL) retreat is the dominant uncertainty in 21st-century projections of global mean sea-level rise (Schoof, 2007; Rignot et al., 2014; DeConto and Pollard, 2016; Millan et al., 2022). The GL marks the transition from grounded to floating ice and migrates inland in response to thinning of the floating shelf and steepening of the bed; its position and migration rate are the most sensitive observable indicators of marine ice-sheet stability.

Differential InSAR has been the workhorse technique for GL detection since Goldstein et al. (1993), and the double-difference InSAR (DDInSAR) variant, in which three SAR acquisitions are configured so that steady ice flow cancels under equal temporal baselines while tidal flexure remains, has become the standard approach (Rignot et al., 2011; Milillo et al., 2017, 2019; Ross et al., 2025b). Recent automated DDInSAR delineation pipelines based on deep learning and phase-gradient analysis on COSMO-SkyMed data (Ross et al., 2024) produce GL position retrievals at sub-monthly cadence, motivating the need for tide-aware acquisition planning to feed those pipelines with the highest-yield triplets. NASA's NISAR mission (NASA-ISRO Synthetic Aperture Radar; Rosen et al., 2017; NASA/ISRO, 2024), in routine Antarctic operations during the first operational year covered by this analysis, is the first open-access L-

https://doi.org/10.5194/egusphere-2026-2542
Preprint. Discussion started: 14 July 2026

band InSAR satellite with the orbital and instrument parameters required for routine Antarctic GL monitoring: a 12-day exact-repeat orbit, SweepSAR design with 240 km coherent imaging swath, ~750 km altitude, and incidence range 33–47°. The 12-day baseline preserves L-band coherence over Antarctic ice; longer baselines typically fail coherence over wind-redistributed snow and dry firn. However, the 12-day repeat closely matches the principal lunar-solar diurnal tide constituent K1 (period 23.93 h) such that 12 d = 12.034 K1 cycles, so the dominant diurnal mode aliases nearly perfectly across the repeat (Padman et al., 2018), and any rigid 12-day triplet samples a tidal envelope that varies by less than 12° of K1 phase per cycle.

Because each 12-day triplet samples a different K1 phase, the predicted DDInSAR fringe count varies by more than an order of magnitude between operationally identical triplets. NISAR's published acquisition plan does not differentiate between high-yield and low-yield triplets at acquisition-scheduling time. The mission's actual policy at the Antarctic coast, confirmed via direct correspondence with the NISAR Project Scientist and Cryosphere Lead, is to acquire every operationally feasible track without culling (P. Rosen, I. Joughin, M. Lavalle, pers. comm., 2026). The geometric ceiling of 240 km imaging swath at −75° latitude limits this to ~9 InSAR-coherent track streams per glacier, so the analyst-facing question is not "which tracks are scheduled?" but "which of the ~300 rigid 12-day triplets per glacier per year are operationally useful for DDInSAR?"

We present tidal-insar-sim, an open-source Python toolkit that answers that question. The library ingests NISAR's operational Reference Observation Plan via the live ArcGIS feature service, auto-discovers all the per-track parameters required for forward DDInSAR modelling, evaluates the CATS2008 ocean-tide model at the exact UT of every scheduled acquisition, enumerates rigid 12-day triplets per InSAR-coherent track stream, and ranks them deterministically by predicted fringe count. The toolkit additionally distinguishes high-tide- from low-tide-at-t_2 acquisition modes, supports continental-scale parameter sweeps, and is generalisable to any SAR or altimetry constellation with a published acquisition plan.

Section 2 develops the DDInSAR forward model at a tidally flexed grounding line. Section 3 describes the toolkit's software architecture and the inputs that are now auto-discovered from the operational ROP rather than manually configured. Section 4 quantifies the NISAR DDInSAR success rate at the three Amundsen Sea Embayment GLs over the first year of operations, confirming the no-culling policy and reporting per-glacier triplet yields. Section 5 quantifies the value of tide-aware ranking under anomaly-driven duty-cycle reductions. Section 6 discusses the synergy with NASA's Surface Topography and Vegetation Designated Observable (STV; Donnellan et al., 2018). Section 7 summarises the open-access release and continental rollout plan.

2 Theory: DDInSAR phase at a tidally flexed grounding line

2.1 Tidal flexure of a floating ice shelf

The tidally driven vertical displacement w(s, t) of a floating ice shelf at distance s downstream of the grounding line, under instantaneous ocean tide h(t) at the GL, follows the elastic-plate solution of Holdsworth (1969):

$$w(s, t) = h(t) \cdot [1 - e^{(-\beta s)} \cdot (\cos\beta s + \sin\beta s)], \quad s \geq 0 \quad (1)$$

with w(s, t) = 0 on the grounded side (s < 0). The flexural parameter $\beta = (\rho_w g / 4 D)^{(1/4)}$ depends on sea-water density ρ_w, gravitational acceleration g, and the flexural rigidity $D = E H^3 / [12 (1 - \nu^2)]$ of the shelf, with E the elastic modulus, H the ice thickness, and ν Poisson's ratio. Default values used by the toolkit are ρ_w = 1028 kg m^{-3}, E = 0.88 GPa, ν = 0.41 (after Sayag and Worster, 2013; Ross et al., 2025a); H is per-site from BedMachine v3 (Morlighem et al., 2020). The flexure decays exponentially with characteristic length π/β; for Thwaites (H ≈ 800 m) this is ≈12 km.

2.2 Double-difference vertical displacement

A DDInSAR triplet at temporal coordinates $t_1 < t_2 < t_3$ with equal temporal baselines $B = t_2 - t_1 = t_3 - t_2$ (the rigid configuration) cancels any displacement field that is linear in time. Steady ice flow contributes $h_{flow}(t) = v\,t$ and therefore produces zero double-difference. Tidal flexure does not cancel because h(t)

https://doi.org/10.5194/egusphere-2026-2542
Preprint. Discussion started: 14 July 2026

is not linear in t; instead the second-order finite difference of w(s, t) survives as the DDInSAR signal. At s = 0 (at the GL itself) the vertical double-difference reduces to the tide double-difference

$$h\_DD = h_1 - 2h_2 + h_3 \quad (2)$$

where h_i = h(t_i) is the local sea-surface elevation at the i-th acquisition. At s > 0 the double-difference inherits the elastic-plate envelope (1) so the spatially resolved DDInSAR phase field is

$$\varphi\_DD(s) = -(4\pi/\lambda) \cdot \cos\theta\_inc \cdot h\_DD \cdot [1 - e^{(-\beta s)}(\cos\beta s + \sin\beta s)] \quad (3)$$

where θ_inc is the incidence angle at the GL and λ the SAR wavelength. The negative sign follows the IEEE radar convention (Bürgmann et al., 2000). The spatial fringe density at the GL is set by |h_DD| and the wavelength; integrating (3) over a flexure half-width gives the line-of-sight fringe count

$$n\_fr = |h\_DD| \cdot \cos\theta\_inc / (\lambda/2) \quad (4)$$

n_fr ≈ 3 is the operational threshold below which the wrapped phase cannot be unambiguously inverted to a flexure profile (Rignot et al., 2011); n_fr ≥ 5 is the regime of excellent SNR where the GL position can be retrieved with sub-pixel precision.

2.3 The K1 aliasing problem

h_DD is most naturally large when the three sea-level samples sit at extreme tidal phases: h_2 near a tidal high while h_1 and h_3 sit at neighbouring lows (or vice versa for the low-tide-at-t_2 mode). Because (2) is sign-symmetric in the triplet, both phase configurations yield equal |h_DD| and therefore equal fringe counts. The operational question is whether NISAR's 12-day cadence can land h_2 at one extreme and $(h_1 + h_3)/2$ at the other. The K1 constituent (period 23.93 h) advances by only ~12° of phase per 12-day step (12 d / 23.93 h = 12.034 K1 cycles), so K1 contributions to all three sea-level samples are nearly identical and cancel in (2). Useful h_DD therefore comes only from the higher-frequency drift of M2, S2 and the compound K1+O1+P1 envelope between cycles. This residual signal varies by more than an order of magnitude across triplets sampled at different absolute K1 phases of the spring tide, motivating tide-aware ranking at the per-triplet level.

3 Software description

3.1 Architecture and data flow

tidal-insar-sim is a pure-Python package targeting Python ≥ 3.10 and is distributed under the MIT licence on PyPI (pip install tidal-insar-sim) and GitHub. Required dependencies are numpy, scipy, pandas, requests, shapely, pyproj, click, and matplotlib; optional dependencies are pyTMD and netCDF4 (live CATS2008 forcing), Skyfield (SGP4 propagation for missions without a published ROP), and streamlit (web UI).

The toolkit's leverages NISAR's operational ROP feature service, which exposes every per-track parameter that earlier versions had to derive from TLE-propagated orbits. Inputs and auto-derived parameters are summarised in Table 1.

https://doi.org/10.5194/egusphere-2026-2542
Preprint. Discussion started: 14 July 2026

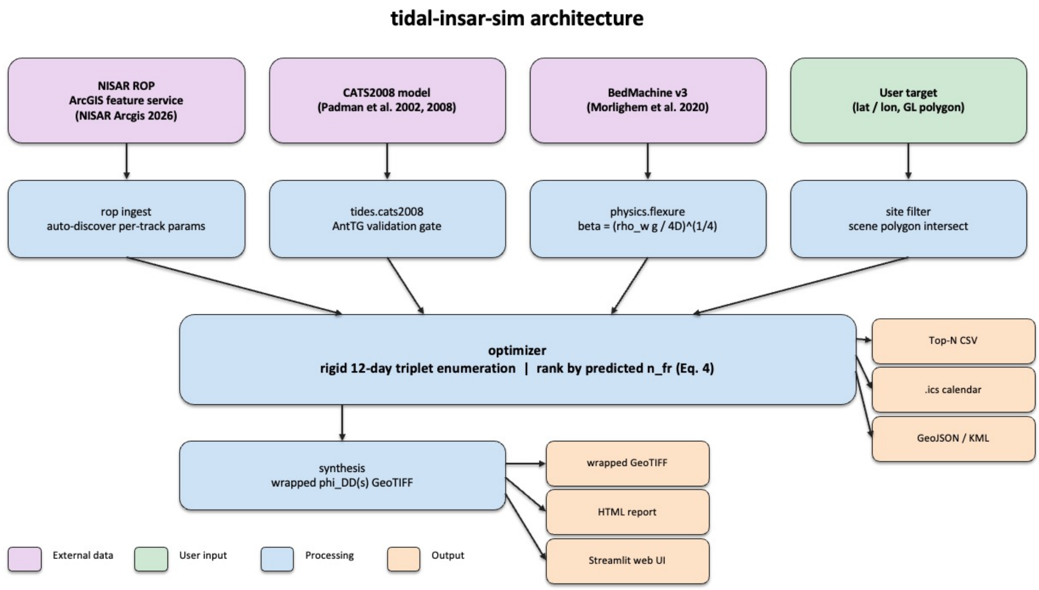

Figure 1. tidal-insar-sim architecture and data flow. External inputs (purple): NISAR Reference Observation Plan ArcGIS feature service, CATS2008 ocean-tide model files, BedMachine v3 ice-thickness grids. User input (green): target lat/lon or grounding-line polygon. Processing modules (blue): rop ingestion with auto-discovery of per-track parameters, site-polygon intersection filter, CATS2008 wrapper with the AntTG validation gate, elastic-plate flexure, the optimizer (rigid 12-day triplet enumerator and ranker), and the synthesis forward model. Outputs (orange): top-N CSV; .ics calendar; GeoJSON / KML footprints; wrapped DDInSAR phase GeoTIFF; HTML report; and an interactive Streamlit web UI.

Field	Source	Used for
Target lat/lon (or GL polygon)	User-supplied	Centroid distance filter; tide evaluation
CATS2008 model files	USAP-DC (Howard & Padman, 2019); auto-installed	Per-acquisition tide elevation
track number	ROP feature.attribute.track	Stream identification
frame number	ROP feature.attribute.frame	Footprint identification
acquisition_time (UT-of-day)	ROP feature.attribute.acquisition_time	Tide evaluation at exact UT
dates (all scheduled cycles)	ROP feature.attribute.dates	Triplet enumeration
pass direction (Asc/Desc)	ROP feature.attribute.passdirection	Look-side and ranking diversity
scene polygon	ROP feature.geometry	Spatial filtering vs target
radar mode mnemonic	ROP feature.attribute.unique_radar_mode_mnemonic_list	Bandwidth, polarisation, swath
polarisation channel	Parsed from mode mnemonic (e.g. SH = single-pol H)	DDInSAR coherence model (future)
bandwidth (40 / 77 MHz)	Parsed from mode mnemonic (e.g. 77M+--- vs 40M+05N)	Range resolution
swath mode (HS / FS)	Parsed from mode mnemonic (HS = half-swath; FS = full-swath)	Cross-track coverage
flexural rigidity D, ice thickness H	BedMachine v3 (Morlighem et al., 2020); user override	Eq. (3) flexure synthesis
usability threshold n_fr*	Default 3; user override	Operational classification

Table 1. Inputs to tidal-insar-sim and the source of each parameter. Parameters previously assumed or derived from TLE propagation (acquisition_time, pass direction, radar mode, bandwidth, swath mode, polarisation) are now

https://doi.org/10.5194/egusphere-2026-2542
Preprint. Discussion started: 14 July 2026

ingested directly from the operational ROP feature service. The toolkit still ships a Skyfield/SGP4 fallback path for missions without a public ROP feature service.

3.2 ROP ingestion and per-track parameter discovery

The rop module wraps the NISAR ArcGIS Online merged-observation-plan feature service (NISAR ArcGIS, 2026). A single spatial query returns every track-frame whose footprint intersects a user-supplied bounding box, with per-feature attributes including the comma-separated list of all scheduled UTC dates, the per-cycle UT-of-day, the pass direction, the polygon footprint geometry, and the full radar mode mnemonic list. The mode mnemonic encodes bandwidth, polarisation, and swath mode in a documented format (e.g. "L:SCI:SH:77M+---:HS:B4:D02" = L-band science mode, single H polarisation, 77 MHz bandwidth, no S-band companion, half-swath beam 4); a parser exposes these as Python attributes.
Direct correspondence with NISAR Cryosphere Lead I. Joughin (pers. comm., 2026) confirmed two operational practices that the toolkit now reads directly rather than assumes: (a) the primary Antarctic L-band mode is 77 MHz half-swath (high SNR, narrow swath) for coastal targets including the ASE GLs studied here; (b) the mission is experimenting with 40 MHz full-swath in interior regions where SNR is lower and full-swath coverage is preferred. Both modes are tagged in the ROP feature service and parsed automatically; downstream stages (the optimiser objective and the synthesis forward model) adjust range resolution and incidence-angle distribution accordingly.

3.3 Tide forcing

CATS2008 ocean-tide values (Padman et al., 2002, 2008, 2018; Howard and Padman, 2019) are extracted at the exact UT of every scheduled acquisition using pyTMD (Sutterley et al., 2024) with the eight default constituents (M2, S2, N2, K2, K1, O1, P1, Q1), 18.6-year nodal correction, and inferred minor constituents enabled. CATS2008 masks grounded ice; grounding-zone sites that fall on a masked cell are remapped to the nearest unmasked ocean cell with a documented <5 km horizontal shift. A runtime validation gate cross-checks the wrapper's M2 and K1 amplitudes against the Antarctic Tide Gauge database (Howard and Padman, 2019) at eight well-calibrated stations within station-specific tolerances of 3–10 cm; any deviation raises CATSValidationError and refuses to run downstream analysis.

3.4 Triplet enumeration and ranking

The optimizer module groups all auto-discovered acquisitions by (track, frame) and enumerates every rigid triplet ($t_1 < t_2 < t_3$) per stream subject to user-configurable constraints (defaults shown): equal-baseline tolerance $|B_1 - B_2| \leq 0.5$ d; central baseline $B \equiv t_2 - t_1 \in [11.5, 12.5]$ d (NISAR's coherence-feasible cadence); maximum span $t_3 - t_1 \leq 30$ d. Each candidate is scored by Eq. (4) with NISAR L-band wavelength $\lambda = 0.238$ m and per-track θ_inc derived from the scene polygon and the orbit altitude. Output is a ranked DataFrame at track-stream level and an .ics calendar of the top-N triplets per glacier ready for ingest into Google Calendar, Outlook, or operational mission-planning systems.

3.5 Forward fringe synthesis and outputs

The synthesis module produces georeferenced wrapped-phase DDInSAR maps from Eq. (3) at user-configurable resolution (default 200 m) in EPSG:3031 polar stereographic projection, loadable directly into QGIS, ISCE2 and GMTSAR. Outputs: ranked CSV; Parquet (site × sensor batch); GeoTIFF wrapped-phase maps; .ics calendars; GeoJSON of footprints; HTML summary reports; PNG figures. A Streamlit web UI exposes the workflow interactively at three pages (Setup, Single Site, Batch).

3.6 Verification and reproducibility

The package ships a 12-module pytest suite covering unit tests of every public API; regression-test snapshots are bit-exact across supported platforms; the package version is embedded in every output file as a metadata field; the CATS2008 wrapper records the model file SHA-256 on first use. Continuous integration on GitHub Actions runs the full suite on Python 3.10–3.13 across Ubuntu, macOS and Windows on every commit; release tags trigger automated deployment to PyPI and Zenodo with a permanent DOI.

https://doi.org/10.5194/egusphere-2026-2542
Preprint. Discussion started: 14 July 2026

4 NISAR DDInSAR success rate over Amundsen Sea grounding lines

4.1 ROP coverage at the ASE coast

We applied the toolkit to derive the predicted DDInSAR yield at the three ASE grounding lines contributing most to current Antarctic mass loss (Thwaites, Pine Island, Smith) over the first year of NISAR operations. The merged ROP feature service was queried for every L-band scene whose footprint intersects the ASE bounding box (−130°→−85° longitude, −78°→−71° latitude); the query returned 199 scenes spanning 58 unique NISAR tracks. Of these, 9 tracks have a frame whose polygon contains Thwaites, 9 contain Pine Island, and 8 contain Smith, the geometric ceiling of NISAR's 240 km imaging swath at −75° latitude (track spacing ~60–70 km at this latitude allows ~4 tracks per side to image any single point within their swath). Direct verification with the NISAR Project Scientist (P. Rosen, pers. comm., 2026) confirmed that every operationally feasible track containing each GL is in the schedule. There is no culling at the Antarctic coast.

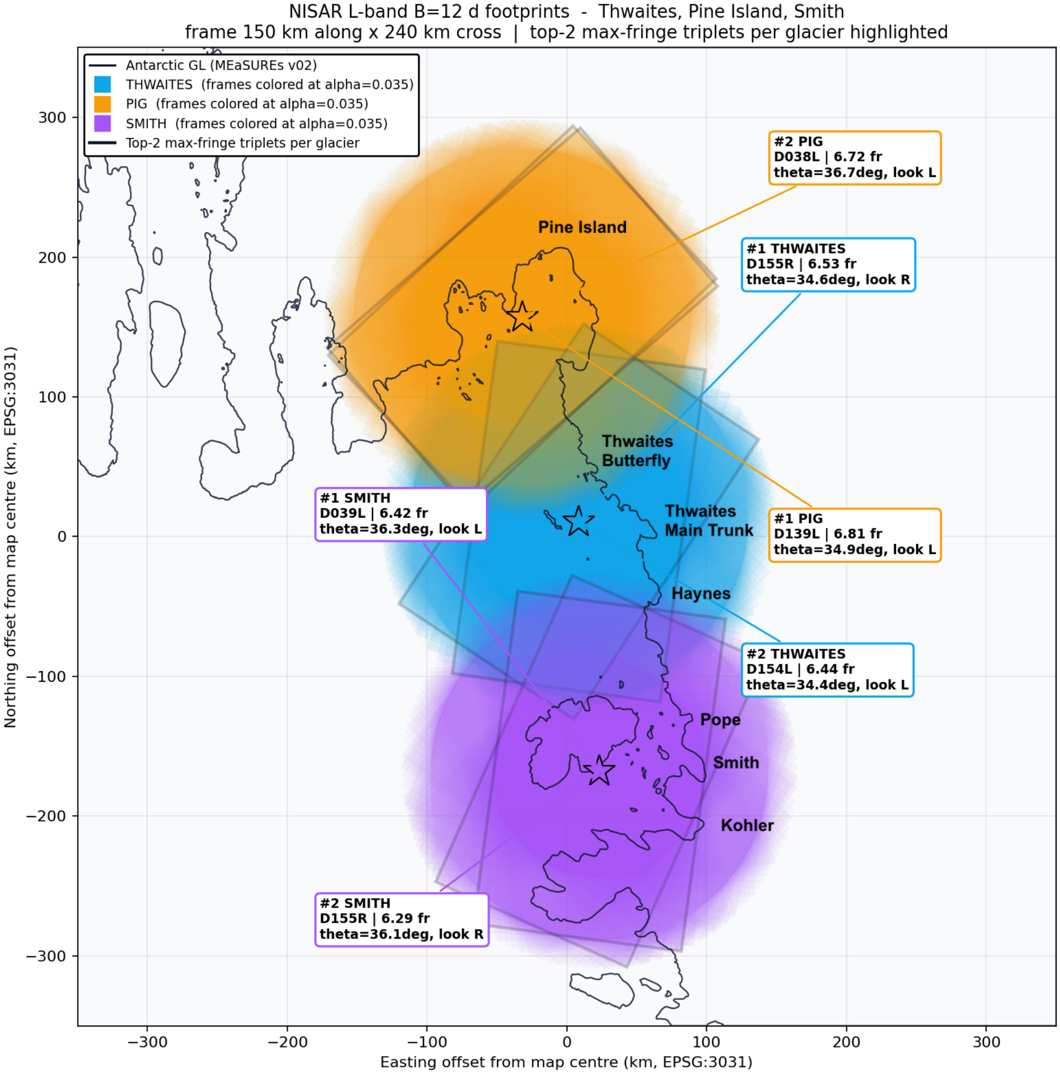

https://doi.org/10.5194/egusphere-2026-2542
Preprint. Discussion started: 14 July 2026

Figure 2. NISAR L-band SAR coverage geometry over the Amundsen Sea grounding-line cluster, generated by tidal-insar-sim from the ROP feature service. Each translucent rectangle is one NISAR SweepSAR footprint (240 × 150 km) oriented along the satellite ground-track heading. Colour encodes the maximum DDInSAR fringe count attainable on that track for an operationally feasible 12-day rigid triplet. Cyan = Thwaites (9 covering tracks), amber = Pine Island (9), purple = Smith (8). Top-2 triplets per glacier highlighted in bold black with call-outs. Solid black: MEaSUREs Antarctic grounding line v02 (Rignot et al., 2016).

4.2 Per-glacier yield and success rate

For every (target, track) combination we read the per-cycle UT-of-day directly from the ROP acquisition_time field, evaluated CATS2008 at the exact UT of every scheduled date, and enumerated rigid 12-day triplets. The first-year window (defined as 365 days from the earliest L-band ASE acquisition in the schedule, 2025-09-24 → 2026-09-24) contains 793 triplets across the three glaciers. The per-glacier breakdown by usability class is reported in Table 2 and Figure 2.

Glacier	Tracks	Triplets	n_fr ≥ 2	n_fr ≥ 3	n_fr ≥ 5	Mean	Max
Thwaites	9	274	75 (27 %)	31 (11.3 %)	3 (1.1 %)	1.49	5.69
Pine Island	9	275	82 (30 %)	28 (10.2 %)	1 (0.4 %)	1.53	5.10
Smith	8	244	68 (28 %)	28 (11.5 %)	1 (0.4 %)	1.47	5.64
ASE total	-	793	225 (28 %)	87 (11.0 %)	5 (0.6 %)	1.50	5.69

Table 2. First-year (Sep 2025 → Sep 2026) NISAR DDInSAR yield over the three Amundsen Sea Embayment grounding lines, from the operational ROP. Triplets are grouped by predicted fringe count: n_fr < 2 unusable, 2≤ n_fr <3 marginal, 3≤ n_fr <5 operational, n_fr ≥ 5 excellent. Mean fringes are 1.5 across all three GLs but the operational success rate is only 11 %; the excellent-quality success rate is 0.6 % (5 triplets per year across the three glaciers).

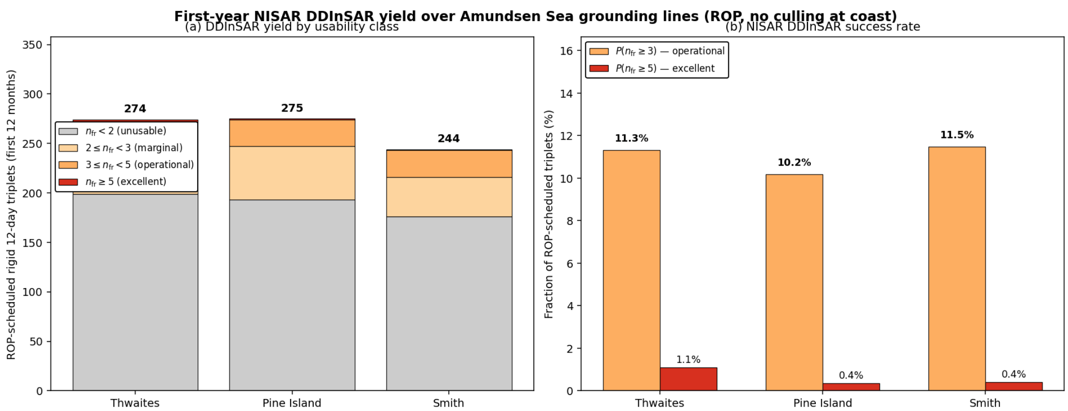

Figure 3. Per-glacier first-year DDInSAR yield over the Amundsen Sea Embayment. (a) Stacked bars decompose total ROP-scheduled rigid 12-day triplets at each GL by usability class; (b) operational and excellent success rates as a fraction of total triplets. The operational success rate is ~11 % at all three glaciers and the excellent-quality success rate is below 1.5 %, despite the schedule including every operationally feasible track. The limit is K1 tidal aliasing at the 12-day repeat, not the schedule.

4.3 Tide-aware ranking and the high vs low t_2 modes

The 87 operational triplets are concentrated in the top quintile of the predicted-fringe-count distribution. Without ranking, an analyst downloading every ROP-scheduled triplet over Thwaites obtains a usable DDInSAR product on roughly one in nine attempts; at Smith, one in nine; at Pine Island, one in ten. With

https://doi.org/10.5194/egusphere-2026-2542
Preprint. Discussion started: 14 July 2026

the ranked list emitted by tidal-insar-sim, the operationally useful triplets are identified up front and the remaining 89 % can be deferred to lower-priority processing pipelines or skipped entirely.

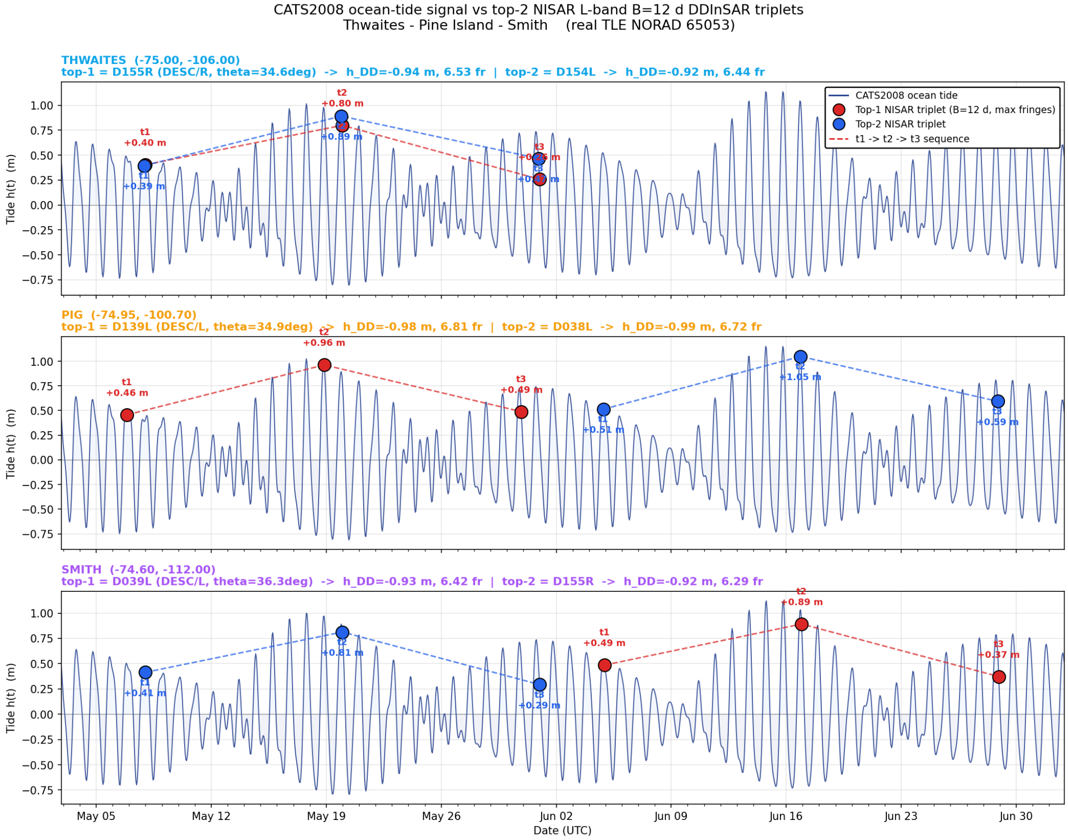

Figure 4. CATS2008 ocean-tide signal versus the top-2 ranked DDInSAR triplets per glacier at Thwaites, Pine Island and Smith over a 60-day window. Red and blue filled circles: top-1 and top-2 ranked triplets at each glacier marked at the exact UT of each acquisition. The optimal triplets share a "spring-tide-at-t_2" pattern with h_2 near a local high tide and h_1, h_3 at neighbouring lows.

The triplet sample is sign-symmetric in h_DD: in the first year, 431 triplets across the three glaciers are high-tide-at-t_2 (h_DD < 0; max 5.69 fringes at Thwaites) and 361 are low-tide-at-t_2 (h_DD > 0; max 4.12 fringes at Thwaites). The two modes cluster in non-overlapping spring-tide windows (May–June 2026 high, January–February 2027 low at Thwaites) and produce DDInSAR retrievals of the same GL position with opposite fringe-rotation sense (Eq. 3). Capturing both modes therefore approximately doubles the count of geometrically independent retrievals at no incremental scheduling cost.

https://doi.org/10.5194/egusphere-2026-2542
Preprint. Discussion started: 14 July 2026

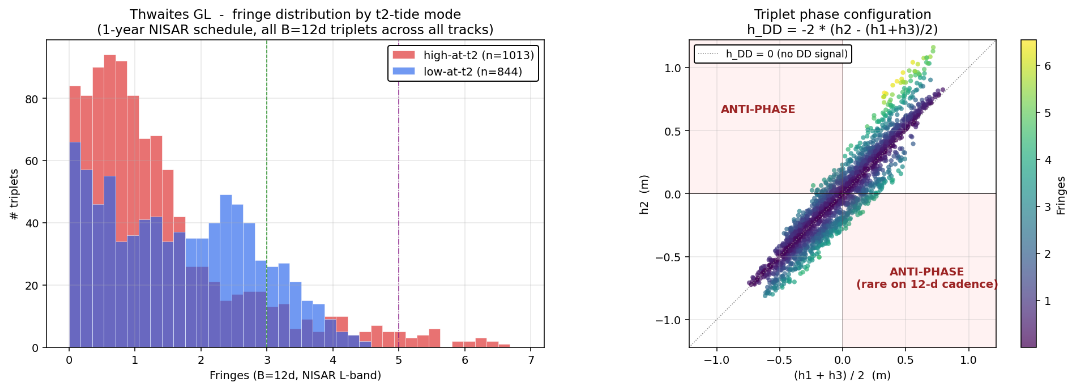

Figure 5. Distribution of DDInSAR fringe-count yield across all rigid 12-day triplets at Thwaites in the first operational year, classified by the sign of h_DD. (a) Histograms of high-tide-at-t_2 (red, h_DD < 0) versus low-tide-at-t_2 (blue, h_DD > 0). Both populations cross the 3-fringe usability threshold at meaningful population fractions; the toolkit retains and ranks both as first-class targets. (b) Scatter of h_2 versus the mean of the bracketing tide samples $(h_1 + h_3)/2$ for every rigid 12-day triplet. The diagonal is the locus where h_DD vanishes (h_2 equals the mean of its neighbours and the second-order finite difference is zero, so no DDInSAR signal develops). Distance from the diagonal is therefore proportional to |h_DD| and gives a direct geometric reading of the strength of every candidate triplet before any tidal forcing model is invoked. Triplets in the upper-right and lower-left quadrants are the high- and low-tide-at-t_2 modes that NISAR's 12-day cadence reaches; the upper-left and lower-right quadrants encode the theoretical anti-phase configuration that would double |h_DD| but is unreachable at the K1-aliased 12-day repeat (sparsely populated, no triplet crosses the threshold). The scatter therefore visualises both the achievable ranking space and the anti-phase upper bound that NISAR's repeat does not access.

4.4 First-year measurement budget

The 87 operational triplets distributed across the first NISAR operational year, broken down by glacier and acquisition date, are shown in Figure 6. The yield is remarkably uniform in time: every glacier returns roughly two operational triplets per month, with the highest concentration in the May to July spring-tide window. Per-glacier counts are 31 at Thwaites, 28 at Pine Island and 28 at Smith, giving an average DDInSAR measurement cadence of approximately 12 days per glacier (one measurement per 12-day repeat cycle). At this cadence the toolkit elevates NISAR's Antarctic GL retreat-rate sensitivity from the multi-month sampling typical of Sentinel-1 12-day pairs to near-continuous biweekly monitoring at the operational $n\_fr \geq 3$ threshold, with five excellent ($n\_fr \geq 5$) retrievals over the year that support sub-pixel GL position retrieval (Rignot et al., 2011; Milillo et al., 2019).

https://doi.org/10.5194/egusphere-2026-2542
Preprint. Discussion started: 14 July 2026

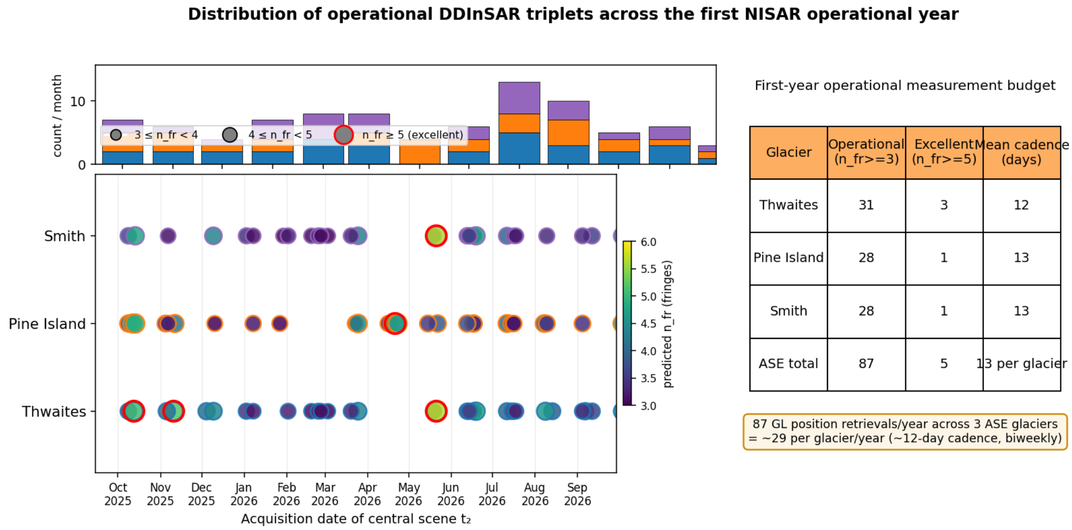

Figure 6. Distribution of the 87 first-year operational DDInSAR triplets (n_fr ≥ 3) across the Amundsen Sea Embayment grounding lines. Top panel: monthly count of operational triplets, stacked by glacier. Main panel: each operational triplet plotted at the UT of its central acquisition t_2, sized and coloured by predicted fringe count; the five n_fr ≥ 5 excellent triplets are circled in red. Right panel: per-glacier measurement budget. The implied cadence is ~29 GL position retrievals per glacier per year, equivalent to one operational DDInSAR measurement per 12-day repeat cycle, an order of magnitude denser than the current Sentinel-1 GL monitoring cadence.

5 Anomaly-response value: tide-aware culling preserves operational yield

NISAR's coastal acquisition policy is uncompromising under nominal operations: every operationally feasible track is acquired, but the mission's power, downlink, and thermal budgets force culling under any anomaly that reduces capability. Single-solar-array faults, polar downlink-station outages, transmitter de-rating, or thermal limits can each force a duty-cycle reduction that propagates to the science scheduler as a per-orbit acquisition cap. Without tide-aware ranking, the planner has no principled basis for choosing which triplets to keep; the default is uniform culling across tracks, which sacrifices a proportional share of the operationally useful triplets.

Because the operationally useful triplets are concentrated in the top quintile of the predicted-fringe-count distribution (Fig. 3a), tide-aware ranked culling preserves operational yield far more efficiently than random culling. We illustrate this for two representative anomaly scenarios: 25 % duty-cycle reduction (e.g. one polar downlink station offline) and 50 % reduction (e.g. one solar-array fault, transmitter de-rated). Under random culling, 25 % of the usable triplets are lost at 25 % cull and 50 % at 50 % cull, in proportion to the duty-cycle reduction. Under tide-aware ranked culling, every one of the 87 first-year ASE usable triplets is retained even at the 50 % anomaly-driven duty-cycle reduction, because the operational gold lives in the top 11 % of triplets and the bottom 50 % is uniformly tide-misaligned. The ranking provides a quantifiable culling budget: the mission can shed up to 89 % of ROP-scheduled ASE triplets in extreme anomaly conditions without losing any operationally useful DDInSAR product.

The same machinery applies in the Antarctic interior, where Joughin (pers. comm., 2026) reports that NISAR acquires with 40 MHz full-swath modes to compensate for the lower SNR of the homogeneous interior surface. Interior culling is real (operational decisions are made about which subglacial lakes, stake networks, and ice-divide sites are imaged on each cycle); the toolkit's per-target ranking provides the same prioritisation framework that the anomaly use case at the coast demonstrates.

6 Synergy with NASA's Surface Topography and Vegetation Designated Observable

https://doi.org/10.5194/egusphere-2026-2542
Preprint. Discussion started: 14 July 2026

The 2017 Decadal Survey for Earth Science (National Academies, 2018) designated Surface Topography and Vegetation (STV) one of five Earth-observing priority areas, with mission concepts subsequently developed by Donnellan et al. (2018, 2024a). STV concept missions including the Earth Dynamics Geodetic Explorer (EDGE) and the Surface deformation and Land Imaging Mission (SLIM; Donnellan et al., 2024b) target sub-metre vertical accuracy of ice-sheet topography from multi-beam laser altimetry and InSAR, with grounding-line monitoring an explicit cryospheric objective.
tidal-insar-sim's tide-aware ranking framework applies to any repeat-pass mission acquiring at the GL: the optimiser is wavelength-agnostic, accepts arbitrary SAR or altimeter look-side geometry, and ranks triplets (or individual repeat passes for altimetry) by predicted vertical double-difference signal under the CATS2008 forcing. A coordinated NISAR-DDInSAR + STV-altimetry campaign at the GL, scheduled on tide-aware criteria from the same upstream tide-model query, produces co-registered ice-thickness change and grounding-line position retrievals at sub-monthly cadence, an unprecedented capability that no single-mission observation plan delivers. Tide-aware acquisition planning also complements ongoing efforts to correct radar-altimeter penetration biases over Antarctic ice (Vashishtha et al., 2025), an explicit science requirement of the STV decadal portfolio. The toolkit ships a generic ConstellationDescriptor abstraction to which any future STV mission's orbit and acquisition specifications can be bound; the TLE-driven Skyfield fallback path used for missions without an operational ROP feature service supports this directly.

7 Discussion and open access

tidal-insar-sim closes a quantifiable gap between NISAR's operational acquisition policy at the Antarctic coast (acquire every operationally feasible track) and the science user's analysis pipeline (download and process every triplet). The per-glacier success rate of 11 % at the n_fr ≥ 3 threshold and 0.6 % at the n_fr ≥ 5 threshold, despite zero culling, establishes that the binding constraint on NISAR's first-year DDInSAR yield over the ASE is K1 tidal aliasing at the 12-day repeat, not the acquisition schedule. The toolkit converts this constraint from an analyst burden into a quantitative ranking that elevates the operationally useful subset of triplets to the top of the request queue.
The package generalises by design: per-track acquisition parameters are ingested directly from the operational ROP feature service (Table 1). Continental rollout to Filchner-Ronne, Ross, Larsen, Amery, Totten and Cook outlets is computationally trivial (~10 s per glacier per year) and is the planned use case for the next release. Cross-mission application to Sentinel-1 (ESA), COSMO-SkyMed (ASI), the upcoming ROSE-L (ESA), and altimetry concepts within the STV portfolio is supported via the Skyfield/SGP4 fallback path (the auto-discovery of per-track parameters relies on the ROP feature service, but the optimiser objective and the synthesis forward model accept any acquisition stream).
tidal-insar-sim v0.3.0 is openly archived on Zenodo at https://doi.org/10.5281/zenodo.20056468 (Milillo, 2026) and released under the MIT licence. Active development continues on GitHub at https://github.com/Milillo-lab/tidal-insar-sim. All scripts to reproduce the figures of this paper are included in the scripts/ directory of the archive along with the ROP feature service URLs and CATS2008 install instructions.

8 Conclusions

We have characterised the predicted DDInSAR success rate of NISAR's first-year operational acquisition plan at the three Amundsen Sea Embayment grounding lines that contribute most to current global mean sea-level rise. Despite the mission's no-culling policy at the Antarctic coast, where every operationally feasible track is scheduled, only 11 % of the resulting rigid 12-day triplets cross the 3-fringe usability threshold and only 0.6 % the 5-fringe excellent-quality threshold, the residual cost of K1 tidal aliasing at the 12-day repeat. tidal-insar-sim, the open-source toolkit described in this paper, ingests the operational ROP feature service directly, auto-discovers every per-track parameter required for forward DDInSAR modelling, evaluates CATS2008 ocean-tide forcing at the exact UT of every scheduled acquisition, and ranks rigid 12-day triplets deterministically by predicted fringe count. Under nominal operations the ranked top-N elevates the operationally useful subset out of the unusable bulk for the analyst; under anomaly-driven duty-cycle reductions of up to 50 % the same ranking preserves 100 % of usable yield by

https://doi.org/10.5194/egusphere-2026-2542
Preprint. Discussion started: 14 July 2026

culling only tide-misaligned triplets. The framework generalises to repeat-track altimetry concepts in NASA's STV Designated Observable portfolio and to other SAR missions with published acquisition plans, and is openly archived for community use.

A practical caveat applies when combining the high-tide-at-t_2 and low-tide-at-t_2 modes into a single grounding-line product. The two modes cluster in non-overlapping spring-tide windows (May to June 2026 high, January to February 2027 low at Thwaites) and are therefore separated in time by several months. Over such intervals, real grounding-line position can evolve through long-period ocean-tide variability and through ice-sheet processes that are themselves modulated by long-period tidal forcing (Milillo et al., 2017, 2022). The CATS2008 regional inverse model includes the Mf, Mm and Ssa long-period constituents but their phase and amplitude have larger uncertainty at sub-monthly to seasonal timescales than the diurnal and semidiurnal cluster, and any joint inversion that combines high-tide and low-tide retrievals should explicitly carry a long-period-tide correction term and propagate its uncertainty into the inferred GL migration rate. We treat this as the natural next step beyond the present ranking-only release; it is not a limitation of the toolkit's per-triplet ranking, which remains agnostic to the multi-month time-window over which retrievals are subsequently combined.

Code and data availability

tidal-insar-sim v0.3.0 is openly archived on Zenodo at https://doi.org/10.5281/zenodo.20056468 (Milillo, 2026) under the MIT licence. Active development continues on GitHub at https://github.com/Milillo-lab/tidal-insar-sim. The NISAR Reference Observation Plan is queried live via the ArcGIS Online feature service at https://services7.arcgis.com/WSiUmUhlFx4CtMBB/arcgis/rest/services/nisar_merged_observation_plans/FeatureServer/0; a snapshot of the query results used for the analysis in this paper is included in the data/rop_snapshot/ directory of the archived release. CATS2008 (Howard and Padman, 2019) is openly available from the U.S. Antarctic Program Data Center (https://doi.org/10.15784/601235). The MEaSUREs Antarctic Grounding Line v02 (Rignot et al., 2016) is available from NSIDC.

Author contributions. PM designed the toolkit, implemented the software, ran the analysis, generated the figures and wrote the paper.

Competing interests. The author declares no competing interests.

Acknowledgements. The author thanks I. Joughin (University of Washington), P. A. Rosen (NASA JPL) and M. Lavalle (NASA JPL) for fruitful discussions and email correspondence on NISAR's operational acquisition plan and on the geometric interpretation of the ROP at high-latitude targets. The author also thanks the developers of pyTMD (T. Sutterley and contributors), Skyfield (B. Crist), and CATS2008 (L. Padman, S. Howard) for the open-source dependencies on which this work depends.

Use of generative AI. *The author used Anthropic's Claude (Sonnet 4.5) as a coding and drafting assistant during the development of tidal-insar-sim and the preparation of this manuscript, including Python code drafts for the orbit, optimizer and ROP-ingest modules, first drafts of selected manuscript paragraphs, figure layout and matplotlib styling. All AI-generated outputs were critically reviewed, edited, validated against the underlying data, code execution and primary references, and revised by the author, who takes full responsibility for the content of the paper and the released software.*

References

https://doi.org/10.5194/egusphere-2026-2542
Preprint. Discussion started: 14 July 2026

Bürgmann, R., Rosen, P. A., and Fielding, E. J.: Synthetic aperture radar interferometry to measure Earth's surface topography and its deformation, Annu. Rev. Earth Planet. Sci., 28, 169–209, 2000.

DeConto, R. M. and Pollard, D.: Contribution of Antarctica to past and future sea-level rise, Nature, 531, 591–597, 2016.

Donnellan, A., Harding, D., Lundgren, P., Wessels, K., Gardner, A., Simard, M., et al.: Designated Observable: Surface Topography and Vegetation. Workshop Report for the National Academies' Decadal Survey of Earth Science, NASA, 2018.

Donnellan, A., Glennie, C., Green, J., Stephen, M., Lundgren, P., Medley, B., Simard, M., Magruder, L., Milillo, P., Lou, Y., Smith, B., Rodgers, M., Lavalle, M., Fladeland, M., Krause, K., Shean, D., Treuhaft, R., and Zinke, R.: NASA's Surface Topography and Vegetation Study, IGARSS 2024, 2259–2261, 2024a.

Donnellan, A., Lundgren, P., Stoker, J., Harding, D., Lefsky, M., Gesch, D., et al.: SLIM: Surface deformation and Land Imaging Mission, mission concept study, NASA Earth Surface Mineral Dust Source Investigation team, 2024b.

Goldstein, R. M., Engelhardt, H., Kamb, B., and Frolich, R. M.: Satellite radar interferometry for monitoring ice sheet motion: application to an Antarctic ice stream, Science, 262, 1525–1530, 1993.

Holdsworth, G.: Flexure of a floating ice tongue, J. Glaciol., 8, 385–397, 1969.

Howard, S. L. and Padman, L.: CATS2008: Circum-Antarctic Tidal Simulation version 2008, U.S. Antarctic Program Data Center, https://doi.org/10.15784/601235, 2019.

Milillo, P., Rignot, E., Mouginot, J., Scheuchl, B., Morlighem, M., Li, X., and Salzer, J. T.: On the short-term grounding zone dynamics of Pine Island Glacier, West Antarctica, Geophys. Res. Lett., 44, 10 436–10 444, 2017.

Milillo, P., Rignot, E., Rizzoli, P., Scheuchl, B., Mouginot, J., Bueso-Bello, J.-L., and Prats-Iraola, P.: Heterogeneous retreat and ice melt of Thwaites Glacier, West Antarctica, Sci. Adv., 5, eaau3433, 2019.

Milillo, P., Rignot, E., Rizzoli, P., Scheuchl, B., Mouginot, J., Bueso-Bello, J.-L., Prats-Iraola, P., and Dini, L.: Rapid glacier retreat rates observed in West Antarctica, Nature Geoscience, 15, 48–53, https://doi.org/10.1038/s41561-021-00877-z, 2022.

Milillo, P.: tidal-insar-sim v0.3.0: an open-source toolkit for tide-aware ranking of NISAR L-band acquisitions over Antarctic grounding lines (software), Zenodo, https://doi.org/10.5281/zenodo.20056468, 2026.

Morlighem, M., Rignot, E., Binder, T., Blankenship, D., Drews, R., Eagles, G., et al.: Deep glacial troughs and stabilizing ridges unveiled beneath the margins of the Antarctic ice sheet, Nat. Geosci., 13, 132–137, 2020.

NASA/ISRO: NASA-ISRO Synthetic Aperture Radar (NISAR) Mission Science Users' Handbook, Jet Propulsion Laboratory, 2024.

NISAR ArcGIS: NISAR Mission Observation Plan, ArcGIS Online merged-observation-plan feature service, https://services7.arcgis.com/WSiUmUhlFx4CtMBB/arcgis/rest/services/nisar_merged_observation_plans/FeatureServer/0, accessed 2026.

National Academies: Thriving on Our Changing Planet: A Decadal Strategy for Earth Observation from Space, National Academies Press, https://doi.org/10.17226/24938, 2018.

Padman, L., Fricker, H. A., Coleman, R., Howard, S., and Erofeeva, L.: A new tide model for the Antarctic ice shelves and seas, Ann. Glaciol., 34, 247–254, 2002.

Padman, L., Erofeeva, S. Y., and Fricker, H. A.: Improving Antarctic tide models by assimilation of ICESat laser altimetry over ice shelves, Geophys. Res. Lett., 35, L22504, 2008.

Padman, L., Siegfried, M. R., and Fricker, H. A.: Ocean tide influences on the Antarctic and Greenland ice sheets, Rev. Geophys., 56, 142–184, https://doi.org/10.1002/2016RG000546, 2018.

Rignot, E., Mouginot, J., and Scheuchl, B.: Antarctic grounding line mapping from differential satellite radar interferometry, Geophys. Res. Lett., 38, L10504, 2011.

Rignot, E., Mouginot, J., Morlighem, M., Seroussi, H., and Scheuchl, B.: Widespread, rapid grounding line retreat of Pine Island, Thwaites, Smith, and Kohler glaciers, West Antarctica, from 1992 to 2011, Geophys. Res. Lett., 41, 3502–3509, 2014.

Rignot, E., Mouginot, J., and Scheuchl, B.: MEaSUREs Antarctic Grounding Line from Differential Satellite Radar Interferometry, Version 2, NASA NSIDC DAAC, https://doi.org/10.5067/IKBWW4RYHF1Q, 2016.

Millan, R., Mouginot, J., Derkacheva, A., Rignot, E., Milillo, P., Ciraci, E., Dini, L., and Björk, A.: Ongoing grounding line retreat and fracturing initiated at the Petermann Glacier ice shelf, Greenland, after 2016, The Cryosphere, 16, 3021–3031, 2022.

Rosen, P. A., Kim, Y., Kumar, R., Misra, T., Bhan, R., and Sagi, V. R.: Global persistent SAR sampling with the NASA-ISRO SAR (NISAR) mission, IEEE Radar Conf., 0410–0414, 2017.

https://doi.org/10.5194/egusphere-2026-2542
Preprint. Discussion started: 14 July 2026

Ross, N., Milillo, P., and Dini, L.: Automated grounding line delineation using deep learning and phase gradient-based approaches on COSMO-SkyMed DInSAR data, Remote Sens. Environ., 315, 114429, 2024.

Ross, N., Milillo, P., Nakshatrala, K., Ballarini, R., Stubblefield, A., and Dini, L.: Importance of ice elasticity in simulating tide-induced grounding line variations along prograde bed slopes, The Cryosphere, 19, 1995–2015, 2025a.

Ross, N., Milillo, P., and Dini, L.: Antarctic grounding line delineation from the Italian Space Agency COSMO-SkyMed DInSAR data, Sci. Data, 12, 1737, 2025b.

Sayag, R. and Worster, M. G.: Elastic dynamics and tidal migration of grounding lines modify subglacial lubrication and melting, Geophys. Res. Lett., 40, 5877–5881, 2013.

Schoof, C.: Ice sheet grounding line dynamics: steady states, stability, and hysteresis, J. Geophys. Res., 112, F03S28, 2007.

Sutterley, T. C., Alley, K., Brunt, K., Howard, S., Padman, L., and Siegfried, M.: pyTMD: Python-based tidal prediction software, Zenodo, https://doi.org/10.5281/zenodo.5555395, 2024.

Vashishtha, A., Milillo, P., Becker Campos, A., Bueso Bello, J. L., Rizzoli, P., and Nilsson, J.: AI-Driven TanDEM-X Penetration Bias Estimation in Antarctica Using ICESat-2 and ECMWF Data: Implications for the NASA Surface Topography and Vegetation Decadal Survey, EGUsphere, 2025, 1–45, 2025.

Vashishtha, A., Milillo, P., Becker Campos, A., Bueso Bello, J. L., Rizzoli, P., and Nilsson, J.: AI-Driven TanDEM-X Penetration Bias Estimation in Antarctica Using ICESat-2 and ECMWF Data: Implications for the NASA Surface Topography and Vegetation Decadal Survey, EGUsphere, 2025, 1–45, 2025.